Article
https://doi.org/10.31489/2024PH4/168-174
UDC537.533.9, 519.245
Received: 10.06.2024
Accepted: 19.08.2024

D.A. Mussakhanov[1*], A.S. Kobey[1], M.G. Golkovsky[2], A.T. Tulegenova[3]

[1]*Institute of Physical and Technical Sciences, L.N. Gumilyov Eurasian National University, Astana 010000, Kazakhstan*
[2]*Budker Institute of Nuclear Physics, SB RAS, 11, Lavrentiev Ave., Novosibirsk 630090, Russia*
[3]*Department of Dosimetry and Physico-Technical Support of Radiation Therapy, Kazakh Institute of Oncology and Radiology, 91 Abay Ave., Almaty 050022, Kazakhstan*
*(*Corresponding author's e-mail: dosymma@gmail.com)*

Dependence of the distribution of absorbed electron flux energy in matter on the beam cross section

Beams of electrons confined in space are widely used in technological operations on welding, cutting, surface treatment. During the passage of electrons in matter, redistribution of beam energy losses occurs. The results of energy loss modeling using the Monte Carlo method presented in this paper demonstrate the redistribution of energy losses in the volume of the substance. There is an increase and then a decrease in energy loss as the electron beam moves deeper into the material. In the direction perpendicular to the beam axis there is an expansion of the energy loss region and then a decrease in the diameter of this region. The presented calculations well explain the results of synthesis of refractory dielectric ceramics. The redistribution of energy losses in the substance determines the morphology of the synthesized samples.

Keywords: synthesis, YAG: Ce ceramics, high-power electron flux, energy loss, Monte Carlo method, Gaussian flux distribution, CASINO V2.5, specific energy losses.

Introduction

High-energy electron fluxes are widely used in a wide variety of applications. Electron fluxes are used for the treatment of oncological diseases [1–4], in tomography [5–10]. Broad electron beams with energies up to tens of megaelectronvolts and narrow focused streams are used for these purposes. Radiation sterilization of medical preparations and medical devices is becoming the main method [11–13]. Widespread especially in recent years electron fluxes have been used for the treatment of products, surface cleaning, welding, cutting. As there are many variants of directions of use, technological electron accelerators of various power and energy of electrons have been created [14–16]. One of the main qualities of electron beam technologies is high efficiency (up to 70–80 %) of conversion of the supplied electrical energy into electron beam energy.

In recent years, attempts have been made to use electron beams for the synthesis of dielectric refractory materials needed for photonics, semiconductor electronics, light sources, and optics. In [17-18] it is shown that by direct impact of a powerful flow of high-energy electrons on the charge of refractory metal oxides it is possible to obtain ceramics in a time less than 1 second, without the use of any other substances to stimulate the process.

Obviously, due to the variety of electron beam applications, which differ in energy, power, and beam geometry, methods of rapid assessment of quantitative characteristics of the energy loss of electron beams as they pass through matter are required. Such methods have been developed and allow predicting quite correctly the distribution of absorbed energy during the passage of electron flow through matter [19-20]. In [21] it is shown that the distribution of energy losses of electron beams of Gaussian shape or limited in cross-section is inhomogeneous. There is a redistribution of energy in the target volume. This effect is very important to take into account when using narrowly directed beams.

The purpose of the present work is to investigate the energy losses of a space-limited flow of high-energy electrons in the volume of irradiated matter.

Modelling methodology

Monte Carlo calculations were performed for beams with a Gaussian flux distribution over the cross section and the number of incident electrons equal to 10 000 and 100 000 at an energy of 1.4 MeV. Water with a density of 1 g/cm^2 and the charge for the synthesis of yttrium-aluminum garnet (YAG) with a density of 1.1 g/cm^2 The CASINO V2.5 software developed at Sherbrooke University [22] was used as an object for energy loss calculations.

The programme does not take into account the effect of inelastic scattering on electron deflection and groups all electron energy loss events into a continuous energy loss function [23]. Under this assumption, the energy between collisions can be calculated using the following equations:

$$E_{i+1} = E_i + \frac{dE}{dS}L \tag{1}$$

$$\frac{dE}{dS} = \frac{-7.85\times10^{-3}\rho}{E_i} \times \sum_{j=1}^{n} \frac{C_j Z_j}{F_j} \ln\left(1.116\left(\frac{E_i}{J_j} + k_j\right)\right) [\text{keV/nm}] \tag{2}$$

where Z_j and J_j are the atomic number and average ionisation potential of element j, respectively. K_j is a variable depending only on Z_j.

The elastic collision angle is determined using pre-calculated values of the partial elastic cross section [24]. For regions containing multiple chemical elements, the atom responsible for electron deflection is determined using the full cross section ratio [25].

Many features were added to the first version of CASINO 2.5 to improve the overall use of modelling. A graphical interface allows the user to view results while the simulation is running to avoid wasting time on simulations with incorrectly specified simulation conditions. A step-by-step wizard guides the user through various dialogue boxes to deflne the sample, set parameters and select the distributions to be created. All simulation data is stored in a single file to simplify the processing of results.

Modeling results

Water and charge for the synthesis of cerium-activated yttrium-aluminium garnet ceramics (YAG: Ce) were chosen as objects for synthesis. Water is the closest medium in terms of absorption capacity to the tissues of living organisms. The charge is used for the radiation synthesis of YAG: Ce ceramics studied with the authors. The electron beam entering the material is scattered by atoms, ions of the substance, transfers its energy to ionisation, generation of secondary electrons. As a result of these processes, as electrons pass through the substance, there is a change in the spatial structure of the beam energy transfer. Part of the energy is transferred to the substance outside the beam cross-section. There is a concentration of energy losses along the beam axis.

Figure 1 shows the results of modelling the distribution of electron energy losses in water as a function of the beam width in water. The lines indicate the boundaries of equal losses indicated in the table. At beam widths from 1 mm to 5 mm, the distribution function has a mushroom shape. As the beam width increases, the general pattern of energy loss distribution approaches a rectangular form. The maximum of the absorbed energy shifts from the surface along the beam. We emphasise that the above results correspond to the distribution of losses in matter of fluxes with equal integral doses.

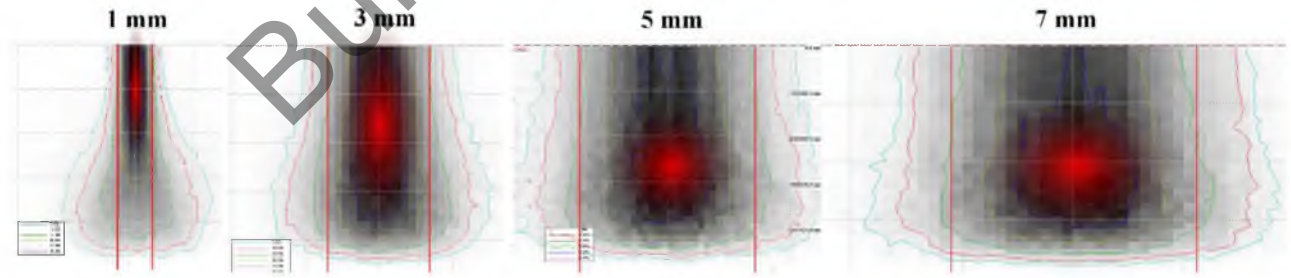

a b c d

Figure 1. Distribution of electron flux energy losses in matter as a function of beam width (a) 1 mm, (b) 3 mm, (c) 5 mm, (d) 7 mm

At the electron flow width of 1 mm, the regions of equal losses have an oval shape. As the electron beam width increases, the areas of maximum energy loss shift along the beam axis, and the oval shape of the energy loss maximum approaches a circular shape.

Figure 2 shows the results of the modelling of energy losses by depth when passing through water. It follows from the presented results that the distribution of energy losses along the beam depth has a complex

character. As the beam passes through, the energy absorption by matter increases, reaches maximum values, and then decreases. The electron travelling depth mainly depends on the electron energy. The influence of the beam width on the energy loss distribution is insignificant. Electrons with energy of 1.4 MeV of beams of different diameters penetrate into water to a depth in the range of 6.4mm-6.6mm.

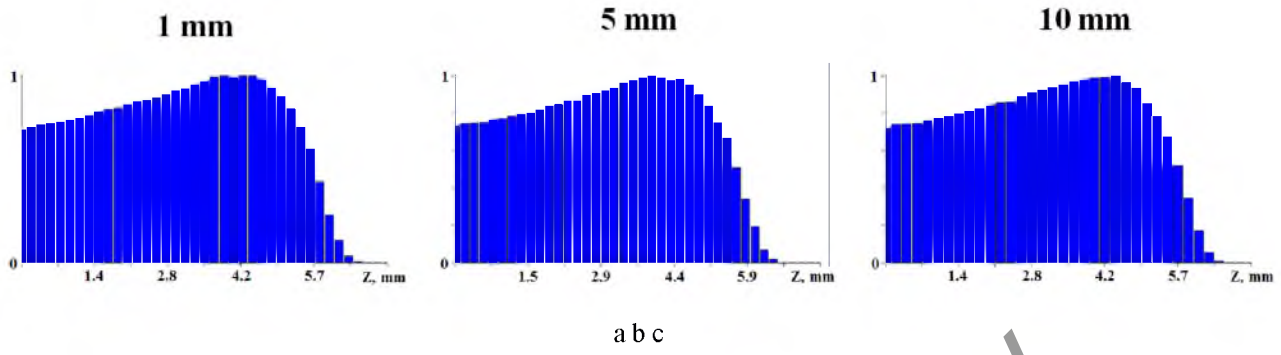

a b c

Figure 2. Electron spacings in matter as a function of beam width(a) 1 mm, (b) 3 mm, (c) 5 mm

Figure 3 shows the energy loss distribution of 1.4 MeV electrons when passing through the charge for YAG synthesis. The charge is a mixture of Al_2O_3 (43 %) and Y_2O_3 (56 %) powders with Ce_2O_3 (1.0 %) as activator. The density of the charge was 1.1 g/cm^2. Calculations were performed by Monte Carlo method using 100 000 iterations. Figure 3 on the left shows the distribution of electron beam energy losses in a cross-section of the irradiated volume along the beam axis. Figure 3 on the right shows the calculated values of electron energy losses in cross sections perpendicular to the beam axis. The coloured lines indicate the boundaries of the energy loss region of equal value indicated in the table.

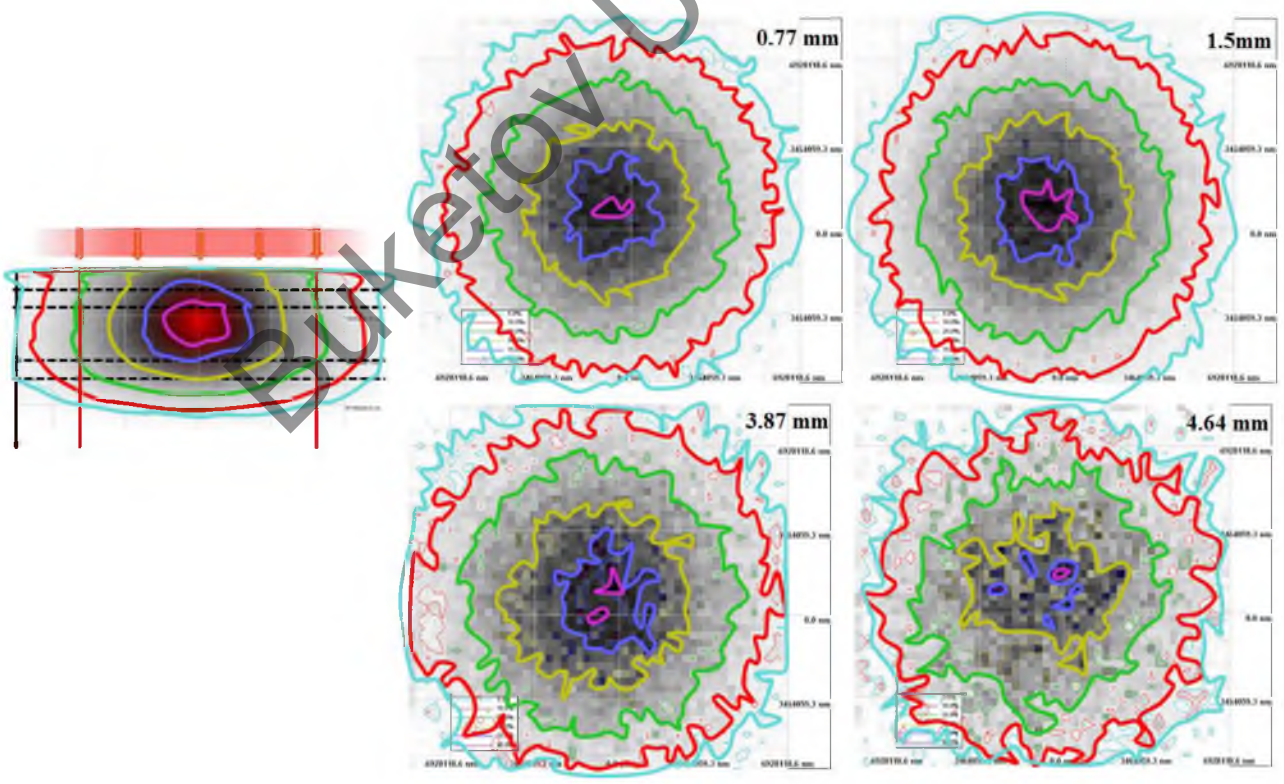

Figure 3. Distribution of electron energy losses along the beam axis and cross sections perpendicular to the beam axis

The maximum electron beam energy losses are near the beam axis. The distribution of specific energy losses in sections perpendicular to the beam axis at depths of 0.77, 1.5, 3.87, and 4.64 mm is similar along

the entire beam path, but differs in absolute value. In general, the energy losses along the beam axis change according to the regularity shown in Figure 2. The losses are maximum in the region of the beam axis. The losses decrease with distance from the axis. In the section perpendicular to the axis, the specific losses are described by a circle with the centre on the axis. However, they differ due to the variation of the cross-sectional diameter of the energy loss region as the beam passes through. The diameter of the circle increases as it moves away from the surface, reaches a maximum value, and then decreases.

Discussion

In order to optimize the modes of radiation synthesis of ceramics, studies of the dependence of the synthesis result on the electron flux power density on the charge surface, which is set in the experiment and well controlled, are carried out. As shown above, the distribution of the absorbed radiation dose is not homogeneous over the irradiated volume both in the depth of the beam passage and in the cross section. The redistribution of absorbed energy in the volume should affect the morphology of the synthesized sample. This effect should certainly be taken into account during synthesis. Therefore, it is necessary to establish a relationship between the electron flux power density on the charge surface and the beam energy losses in the irradiated region of the charge. To establish the relationship, we introduce the following definitions: integral electron beam power density and specific beam energy losses in the charge volume. Under integral we will understand the power density averaged over the entire beam area on the charge surface P_I. Under specific energy losses we will understand the energy losses of the electron flux in the unit of elementary volume W_L in the irradiated area of the material with given coordinates.

For the synthesis of ceramics in the field of high-energy electron flow in [17-18], a Gaussian electron beam with a diameter of 1.2 cm was usually used on the surface of the charge with an area of about 1 cm^2. The energy loss is maximum along the axis of the beam passing through the medium along the entire electron flow path. Along the beam axis, the energy loss increases, then decreases to 0 (Fig. 2). Energy losses along the beam axis are maximum at some depth from the surface, depending on the electron energy and absorption capacity of the substance. In the cross-section transverse to the axis, the energy losses of the electron flow decrease from the maximum on the beam axis to 0. The diameter of the specific energy loss distribution area grows along the beam axis to the maximum, then decreases. The distribution of specific energy losses in the cross-section of the beam has a bell-shaped form similar to the one shown in Figure 4.

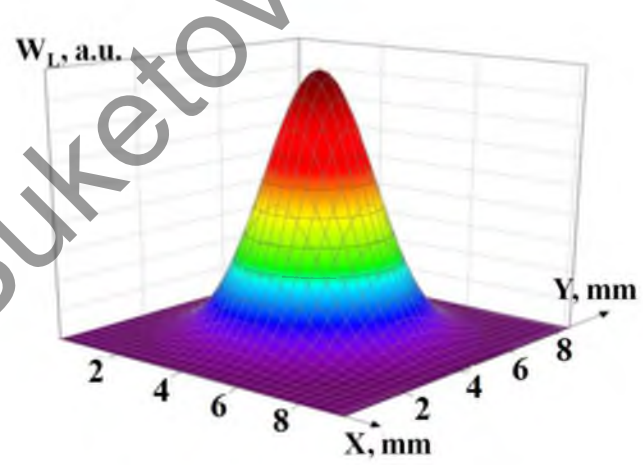

Figure 4. Distribution of specific energy losses of electron flow in the cross-section perpendicular to the beam axis

This distribution of specific losses is qualitatively similar for all modes of radiation exposure at the same experiment geometry and electron energy. With increasing integral power density, only absolute values of specific losses grow proportionally, but the picture does not change qualitatively. Specific energy losses in the whole volume of irradiated matter also grow proportionally.

In order to form ceramics in the radiation field it is necessary to overcome the threshold for the realisation of this process. Synthesis is realised in those areas of the charge in which specific energy losses of the radiation flux exceed this threshold. Therefore, the morphology of the sample obtained by the radiation method reflects the distribution of energy losses.

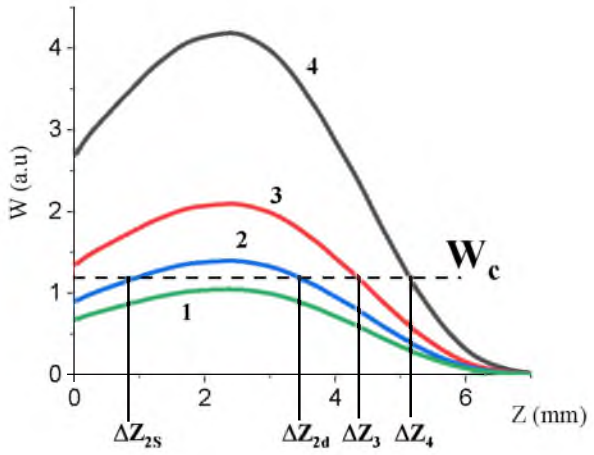

Figure 5. Distribution of specific energy losses of electron flux along the beam axis

Figure 5 shows the results of calculations of the values of specific energy losses of the electron flux with energy of 1.4 MeV along the beam axis in the charge. The results are presented in relative units of integral values of the electron flux power density $W_{L,\,a.u.}$ at the same exposure time, differing in the ratio 4:3:2:1. The dotted line indicates the value of the threshold of specific electron flux energy losses W_c, sufficient to realise the synthesis. Synthesis is realised in those regions where specific electron flux energy losses are sufficient or exceed the threshold. Synthesis is not realised at $W_{L,\,a.u.}$ (1), it is realised on the electron flow path with $W_{L,\,a.u.}$ (3), $W_{L,\,a.u.}$ (4) in the range from 0 to ΔZ_3 and ΔZ_4, respectively, as well as in the range from ΔZ_{2s} to ΔZ_{2d} at $W_{L,\,a.u.}$ (2). This explains the experimentally observed facts. At small values of the integral power density of the electron flux, fusion is realised in the subsurface layer. The thickness of the synthesised ceramics increases with increasing integral electron flux power density.

Acknowledgements

This research has been/was/is funded by the Science Committee of the Ministry of Science and Higher Education of the Republic of Kazakhstan (Grant No. AP23490986)

This research was funded by the Ministry of Trade and Integration of the Republic of Kazakhstan (Grant No. BR12967832)

References

1 Voogt, E. L. K., van Rees, J. M., Hagemans, J. A. W., Rothbarth, J., Nieuwenhuijzen, G. A. P., Cnossen, J. S., Peulen, H. M. U., Dries, W. J. F., Nuyttens, J., Kolkman-Deurloo, I.-K., Verhoef, C., Rutten, H. J. T., & Burger, J. W. A. (2021). Intraoperative electron beam radiation therapy (IOERT) versus high-dose-rate intraoperative brachytherapy (HDR-IORT) in patients with an R1 resection for locally advanced or locally recurrent rectal cancer. *International Journal of Radiation Oncology*Biology*Physics*, *110*(4), 1032–1043. https://doi.org/10.1016/j.ijrobp.2021.02.006

2 Kurokawa, C. (2023). 3 physics for electron beam therapy. *Japanese Journal of Radiological Technology*, *79*(10), 1194–1199. https://doi.org/10.6009/jjrt.2023-2264

3 Sehrish Abrar, Bilal Mazhar Qureshi, Asim Hafiz, Nasir Ali, Agha Mohammad Hammad Khan, & Ahmed Nadeem Abbasi (2022). Total skin electron beam therapy (TSEBT) in management of mycosis fungoides: A case series. *Journal of the Pakistan Medical Association*. https://doi.org/10.47391/jpma.3784

4 Tavallaie, M., Hariri Tabrizi, S., & Heidarloo, N. (2022). Implementation of pencil beam redefinition algorithm (PBRA) for intraoperative electron radiation therapy (IOERT) treatment planning. *Physica Medica*, *104*, 32–42. https://doi.org/10.1016/j.ejmp.2022.10.015

5 Gan, L., & Jensen, G. J. (2011). Electron tomography of cells. *Quarterly Reviews of Biophysics*, *45*(1), 27–56. https://doi.org/10.1017/s0033583511000102

6 Koike, T., & Yamada, H. (2018). Methods for array tomography with correlative light and electron microscopy. *Medical Molecular Morphology*, *52*(1), 8–14. https://doi.org/10.1007/s00795-018-0194-y

7 Wan, W., & Briggs, J. A. G. (2016). Cryo-electron tomography and subtomogram averaging. *Methods in Enzymology*, 329–367. https://doi.org/10.1016/bs.mie.2016.04.014

8 Bárcena, M., & Koster, A. J. (2009). Electron Tomography in life science. *Seminars in Cell & Developmental Biology*, *20*(8), 920–930. https://doi.org/10.1016/j.semcdb.2009.07.008

9 Zheng, T., & Cai, S. (2024). Recent technical advances in cellular cryo-electron tomography. *The International Journal of Biochemistry & Cell Biology*, *175*, 106648. https://doi.org/10.1016/j.biocel.2024.106648

10 Wu, Y. C., Zhu, B., Li, G., Zhang, X. H., Yu, M. H., Dong, K. G., Zhang, T. K., Yang, Y., Bi, B., Yang, J., Yan, Y. H., Tan, F., Fan, W., Lu, F., Wang, S. Y., Zhao, Z. Q., Zhou, W. M., Cao, L. F., & Gu, Y. Q. (2018). Towards high-energy, high-resolution computed tomography via a laser driven micro-spot gamma-ray source. *Scientific Reports*, *8*(1). https://doi.org/10.1038/s41598-018-33844-7

11 Sharifi, S., Sharifi, H., Guild, C., Islam, M. M., Tran, K. D., Patzer, C., Dohlman, C. H., Paschalis, E. I., Gonzalez-Andrades, M., & Chodosh, J. (2021). Toward electron-beam sterilization of a pre-assembled Boston keratoprosthesis. *The Ocular Surface*, *20*, 176–184. https://doi.org/10.1016/j.jtos.2021.02.009

12 Sharifi, S., Islam, M. M., Sharifi, H., Islam, R., Huq, T. N., Nilsson, P. H., Mollnes, T. E., Tran, K. D., Patzer, C., Dohlman, C. H., Patra, H. K., Paschalis, E. I., Gonzalez- Andrades, M., & Chodosh, J. (2021). Electron beam sterilization of poly(methyl methacrylate)—physicochemical and biological aspects. *Macromolecular Bioscience*, *21*(4). https://doi.org/10.1002/mabi.202000379

13 Wilińska, J., Turek, A., Borecka, A., Rech, J., & Kasperczyk, J. (2019). Electron beam sterilization of implantable rods with risperidone and with 17-β-estradiol: a structural, thermal and morphology study. *Acta of Bioengineering and Biomechanics*, *21*(3), 39–47.

14 Ulakhanov, N. S., Mishigdorzhiyn, U. L., Shin, V. I., Moskvin, P. V., Mokeev, M. A., Vorobyov, M. S., & Tikhonov, A. G. (2024). Electron beam treatment of diffusion B–al layers on 3Kh2V8F steel surfaces. *Bulletin of the Russian Academy of Sciences: Physics*, *88*(4), 664–670. https://doi.org/10.1134/s1062873823706347

15 Egorov, I.S., Kaikanov, M.I., Lukonin, E.I., Remnev, G.E., & Stepanov, A.V. (2013). The astra repetitive-pulse electron accelerator. *Instruments and Experimental Techniques*, *5*, 81–84. DOI: https://doi.org/10.7868/s0032816213050030

16 Vorobyov, M. S., Ivanov, Y. F., Akhmadeev, Y. H., Moskvin, P. V., Petrikova, E. A., & Lopatin, I. V. (2018). Surface structure and properties of high-chromium steel irradiated with a submillisecond pulsed electron beam. *Journal of Physics: Conference Series*, *1115*, 032064. https://doi.org/10.1088/1742-6596/1115/3/032064

17 Lisitsyn, V., Tulegenova, A., Golkovski, M., Polisadova, E., Lisitsyna, L., Mussakhanov, D., & Alpyssova, G. (2023). Radiation synthesis of high-temperature wide-bandgap ceramics. *Micromachines*, *14*(12), 2193. https://doi.org/10.3390/mi14122193

18 Lisitsyn, V., Tulegenova, A., Kaneva, E., Mussakhanov, D., & Gritsenko, B. (2023). Express synthesis of YAG:CE ceramics in the high-energy electrons flow field. *Materials*, *16*(3), 1057. https://doi.org/10.3390/ma16031057

19 Tabata, T., Andreo, P., & Shinoda, K. (1998). An algorithm for depth–dose curves of electrons fitted to Monte Carlo data. *Radiation Physics and Chemistry*, *53*(3), 205–215. https://doi.org/10.1016/s0969-806x(98)00102-9

20 Tatsuo, T., Pedro, A., Kunihiko, S., & Rinsuke, I. (1994). Energy deposition through radiative processes in absorbers irradiated by electron beams. *Nuclear Instruments and Methods in Physics Research Section B: Beam Interactions with Materials and Atoms*, *93*(4), 447–456. https://doi.org/10.1016/0168-583x(94)95633-2

21 Lisitsyn, V., Mussakhanov, D., Tulegenova, A., Kaneva, E., Lisitsyna, L., Golkovski, M., & Zhunusbekov, A. (2023). The optimization of Radiation Synthesis Modes for YAG:CE Ceramics. *Materials*, *16*(8), 3158. https://doi.org/10.3390/ma16083158

22 Joly, D., Poirier-Demers, N., & Demers, H. (2011). *Casino 3.2 user manual*. Casino 3.2 User Manual. https://casino.espaceweb.usherbrooke.ca/fichiers/User_Manual_Casino_3.2.pdf

23 Joy, D. C., & Luo, S. (1989). An empirical stopping power relationship for low- energy electrons. *Scanning*, *11*(4), 176–180. https://doi.org/10.1002/sca.4950110404

24 Drouin, D., Hovington, P., & Gauvin, R. (1997). Casino: A New Monte Carlo Code in C language for electron beam interactions—part II: Tabulated values of the Mott Cross section. *Scanning*, *19*(1), 20–28. https://doi.org/10.1002/sca.4950190103

25 Hovington, P., Drouin, D., & Gauvin, R. (1997). Casino: A New Monte Carlo Code in C language for electron beam interaction — part I: Description of the program. *Scanning*, *19*(1), 1–14. https://doi.org/10.1002/sca.4950190101

Д.А. Мусаханов, А.С. Көбей, М.Г. Голковский, А.Т. Тулегенова

Электрон ағыны энергиясының заттағы сіңірілуінің таралуының сәуле көлденең қимасына тәуелділігі

Кеңістікте шектелген электрон сәулелері дәнекерлеу, кесу, бетті өңдеу сияқты технологиялық операцияларда кеңінен қолданылады. Электрондардың зат арқылы өтуі кезінде сәуле энергиясының шығындары қайта бөлінеді. Осы жұмыста Монте-Карло әдісін қолдана отырып ұсынылған энергия шығынын модельдеу нәтижелері зат көлеміндегі энергия шығынын қайта бөлуді көрсетеді. Электрон сәулесі материалға тереңірек енген сайын энергия шығынының артуы және кейіннен кемуі байқалады. Сәуле осіне перпендикуляр бағытта энергия шығыны аймағының кеңеюі және кейіннен осы аймақтың диаметрінің азаюы байқалады. Ұсынылған есептеулер отқа төзімді диэлектрлік керамиканы синтездеу нәтижелерін жақсы түсіндіреді. Заттағы энергия шығындарының қайта бөлінуі синтезделген үлгілердің морфологиясын анықтайды.

Кілт сөздер: синтез, YAG:Ce керамикасы, жоғары қуатты электрон ағыны, энергия шығыны, Монте-Карло әдісі, Гаусс ағынының таралуы, CASINO V2.5, меншікті энергия шығындары.

Д.А. Мусаханов, А.С. Кобей, М.Г. Голковский, А.Т. Тулегенова

Зависимость распределения поглощенной энергии потока электронов в веществе от поперечного сечения пучка

Пучки электронов, ограниченные в пространстве, широко используются в технологических операциях сварки, резки и обработки поверхности. При прохождении электронов в веществе происходит перераспределение потерь энергии пучка. Результаты моделирования потерь энергии с использованием метода Монте-Карло, представленные в данной работе, демонстрируют перераспределение потерь энергии в объеме вещества. Наблюдается увеличение, а затем уменьшение потерь энергии по мере углубления электронного пучка в материал. В направлении, перпендикулярном оси пучка, происходит расширение области потерь энергии, а затем уменьшение диаметра этой области. Представленные расчеты хорошо объясняют результаты синтеза тугоплавкой диэлектрической керамики. Перераспределение потерь энергии в веществе определяет морфологию синтезированных образцов.

Ключевые слова: синтез, керамика YAG:Ce, высокомощный поток электронов, потери энергии, метод Монте-Карло, гауссово распределение потока, CASINO V2.5, удельные потери энергии.

Information about the authors

Mussakhanov D.A. (corresponding author) — Candidate of technical sciences, Senior teacher, Institute of Physical and Technical Sciences, L.N. Gumilyov Eurasian National University, Astana 010000, Kazakhstan; e-mail: *dosymma@gmail.com*, ORCID ID: 0000-0002-1823-2526

Kobey Abylay — PhD student, Institute of Physical and Technical Sciences, L.N. Gumilyov Eurasian National University, Astana 010000, Kazakhstan; e-mail: kobeyablay@gmail.com, ORCID ID: https://orcid.org/0009-0005-8707-4671

Golkovski M.G. — Candidate of physical and mathematical sciences, Senior researcher, Budker Institute of Nuclear Physics, Academician Lavrentiev avenue, 11, Novosibirsk, Russia, e-mail: *golkovski@mail.ru*. ORCID ID: https://orcid.org/0000-0003-4399-444X

Aida Tulegenova — Candidate of physical and mathematical sciences, Acting assistant professor, Institute of Applied Science & Information Technology, al-Farabi Kazakh National University, Almaty, Kazakhstan; e-mail: *tulegenova.aida@gmail.com*; https://orcid.org/0000-0002-5701-6674